Coastal groundwater level trends reveal global susceptibility to seawater intrusion

Annika Nolte[1,2*], Steffen Bender[1], Jens Hartmann[2], Stefan Baltruschat[2], Nils Moosdorf[3,4], Robert Reinecke[5]

[1]Climate Service Center Germany (GERICS), Helmholtz-Zentrum Hereon, Hamburg, Germany

[2]Institute for Geology, Universität Hamburg, Hamburg, Germany

[3]Leibniz Centre for Tropical Marine Research (ZMT), Bremen, Germany

[4]Institute of Geosciences, Kiel University, Kiel, Germany

[5]Institute of Geography, Johannes Gutenberg University Mainz, Mainz, Germany

*Corresponding author

Abstract

Coastal groundwater is a vital freshwater source threatened by overabstraction and sea-level rise, yet global patterns of declining groundwater levels (GWLs) and susceptibility to seawater intrusion (SWI) remain poorly constrained. Here, we present the first global assessment based on in-situ observations from ~480,000 coastal monitoring locations. From 1990 to 2024, 21% of grid-cell aggregates had significant rising or falling GWL trends with magnitudes ≥0.1 m yr^{-1} and with declines becoming more frequent in the last 9 years. More pronounced changes are observed for deeper water tables (ρ_s=0.63), in arid settings (ρ_s=0.56), and in some rural areas. SWI susceptibility is higher where seaward freshwater discharge is weak or gradients reverse landward, leaving limited hydraulic resistance to SWI. Decadal trend extrapolation suggests that these conditions mostly persist (93.4%), while 3.5% newly emerge and 3.1% stabilize (gradients strengthen seaward). The results provide global evidence for prioritizing monitoring and management of coastal groundwater at risk of salinization.

Introduction

Groundwater is a critical freshwater source in coastal regions, which are home to 2.86 billion people (Cosby et al., 2024), and plays a vital role in sustaining coastal ecosystems and their services (Dyring et al., 2022; Luijendijk et al., 2020) as well as marine biota (Lecher and Mackey, 2018). However, coastal aquifers face pressure from growing coastal populations (Neumann et al., 2015), and are increasingly vulnerable to seawater intrusion (SWI), which threatens both the quantity and quality of available water. Salinization reduces water suitability for human use. It has adverse health impacts when drinking-water salinity increases (Mueller et al., 2024), threatens agriculture by lowering soil fertility and crop yields when salinity of irrigation water increases (Ghirardelli et al., 2024), and affects coastal ecosystems, where increased salinity can stress vegetation and soil communities and lead to shifts in species composition (Venâncio et al., 2022; Tully et al., 2019). Climate change and, as a consequence, sea-level rise, changes in groundwater recharge, and intensifying water use increase pressure on coastal groundwater systems (IPCC, 2021; Spinoni et al., 2021; Richardson et al., 2024). This makes it increasingly important to identify where coastal groundwater resources are susceptible to SWI and where monitoring and management should focus to detect and respond to emerging threats.

In coastal settings, hydraulic gradients at the land-sea boundary govern the balance between fresh submarine groundwater discharge and the intrusion of seawater into the nearshore aquifer. Persistent landward or near-zero seaward gradients therefore favor lateral SWI and constitute a first-order control on coastal

groundwater-ocean exchange (Werner et al., 2012; Werner, 2017; Kretschmer et al., 2025b). Here, we use the hydraulic gradient as a scalable proxy for whether freshwater tends to discharge seaward or seawater tends to intrude landward. Gradients summarize coastal head differences and thus integrate the effects of multiple controls. Aquifer properties and architecture, including surface-water connectivity, modulate how natural recharge, human pressures (e.g., groundwater abstraction, land drainage, land-surface changes that modify recharge, sea-level rise) and sea-level rise translate into gradients (Kretschmer et al., 2025b). In particular, two natural settings predispose coasts to landward or near-zero seaward gradients by constraining freshwater heads: topography-limited low-relief coastal plains and recharge-limited (often arid and water-limited) settings (Michael et al., 2013). In topography-limited settings, freshwater heads are already close to the land surface, leaving limited capacity for further head increase under sea-level rise. In recharge-limited settings, limited replenishment suppresses freshwater heads and constrains head recovery. Here, long groundwater response times (hydraulic memory) can delay and buffer responses to climate variability, even as water-table sensitivity to recharge or precipitation can be high and increase with aridity (Fan et al., 2023; Cuthbert et al., 2019). Projected aridification and shifting precipitation regimes are expected to further reduce recharge in recharge-limited coasts, increasing SWI susceptibility (Richardson et al., 2024).

Yet despite our general process understanding, the global spatiotemporal distribution of SWI-susceptible conditions remains poorly characterized. This limits our ability to anticipate where and how salinization pressures may intensify under future climatic and anthropogenic change and reflects broader limitations in global groundwater assessments, which often lack the resolution, integration, and observational grounding needed to capture the complexity of groundwater systems (Gleeson et al., 2020). Most assessments of coastal groundwater systems are focused on local or regional case studies (e.g., Morgan and Werner, 2015; Costall et al., 2020), which presents challenges of commensurability when seeking a better understanding about global-scale processes (Gleeson et al., 2021). Global approaches to model SWI (Adams et al., 2024; Zamrsky et al., 2024; Kretschmer et al., 2025a) continue to face high uncertainties due to assumptions concerning boundary conditions and hydrogeological parameterization, and are challenging to evaluate due to the coarse spatial resolution and spatially-biased availability of time-varying GWL data (Gleeson et al., 2021; Reinecke et al., 2024). GRACE (Gravity Recovery and Climate Experiment) satellite observations provide valuable information for major groundwater basins. However, coarse spatial resolution, land-ocean leakage near coasts, and the residual-based derivation of groundwater storage changes from model-partitioned water components can yield physically implausible estimates and limit applicability, particularly for smaller or coastal systems (Frappart and Ramillien, 2018; Costantini et al., 2023; Arifin et al., 2025).

In contrast, key indicators of coastal groundwater susceptibility to SWI can be derived from in-situ GWL observations, specifically hydraulic heads that favor lateral SWI and declining GWLs that lower freshwater

heads (Kretschmer et al., 2025a; Ferguson and Gleeson, 2012; Jasechko et al., 2020). However, GWLs remain difficult to integrate at scale due to fragmented responsibilities, limited digitization, accessibility issues, and non-standardized datasets (United Nations, 2022; Famiglietti and Rodell, 2013; Lall et al., 2020). Despite these challenges, few efforts have leveraged large-sample in-situ GWL data. Fan et al. (2013) were the first to compile GWL observations globally. This was the basis for developing modeled estimates of water table depth (WTD) with global coverage (e.g., Ma et al., 2024; Fan et al., 2013), now widely used in groundwater-related environmental studies (e.g., Shokri-Kuehni et al., 2020). Recent in-situ syntheses have quantified GWL trends across terrestrial aquifer systems globally (Jasechko et al., 2024) and regionally in southwestern Europe (Chávez García Silva et al., 2024), but without a specific coastal focus. By contrast, Jasechko et al. (2020) focused on coastal areas but limited their analysis to the contiguous United States, while Nolte et al. (2024) used thousands of globally distributed coastal GWL time series to identify common GWL dynamics and highlight limitations of global datasets in explaining these patterns, without deriving GWL trends or explicitly assessing susceptibility to SWI. Collectively, these studies underscore both the value of in-situ GWL data and the persistent gap in globally integrated, observation-based assessments of coastal aquifers. Here, we compile an unprecedentedly large and diverse global set of in-situ coastal GWL observations to derive land-sea hydraulic gradients and recent trends summarized on a common spatial grid for global mapping as observation-based indicators of SWI susceptibility, and to examine how these indicators vary across aridity conditions and coastal regions worldwide.

Susceptible hydroclimatic conditions

Hydroclimatic susceptibility to lateral SWI in our framework is defined by two variables: the land-sea hydraulic gradient that we use as an observation-accessible screening diagnostic, and aridity as a practical proxy for natural recharge limitation. We quantify the land-sea gradient as the change in hydraulic head between inland monitoring locations and the coastline, divided by their distance to the coastline, and classify it as "flat" when it is landward or weakly seaward ($\leq 10^{-3}$ m m^{-1}). This "flat-gradient" class favors lateral SWI (Kretschmer et al., 2025a; Ferguson and Gleeson, 2012). All remaining gradients are grouped as steep ($>10^{-3}$), representing stronger seaward head gradients that generally oppose inland SWI. While this steep class spans a wide range of seaward conditions, we use this binary split as a simple, transparent global screening. Aridity is represented by the aridity index (AI; the ratio of precipitation to potential evapotranspiration; Zomer et al., 2022), with water-limited climates (AI≤1; rather dry) contrasted against energy-limited climates (AI>1; rather wet). The combination of flat gradients and water-limited climates forms the most susceptible hydroclimatic cluster (C1) in our analysis (Fig. 1; compare Methods). Water table depth (WTD) provides important context because shallow groundwater implies limited vadose storage, so modest declines can more readily weaken land-sea gradients and increase salinization risk. Globally,

aquifers near coasts are often shallow: the median coastal WTD is 6.1 m, and nearly half of all observations are shallower than 5 m (Supplementary Material A). Flat gradients, which weaken the natural flow of groundwater toward the sea, are found in about one-third of all observed coastal areas. Although steeper gradients dominate overall (skewed distribution in Fig. 1a), flat gradients remain common even tens of kilometers inland (34-37% of all observations; Fig. 1c). Compared to the global aridity distribution of coastal regions, our dataset shows a distinct clustering near the transitional AI value of approximately 1 (marking the boundary between water- and energy-limited climates), a zone in which groundwater recharge is expected to be particularly sensitive to modest shifts in long-term aridity (Berghuijs et al., 2024). In contrast, moderately arid regions (AI~0.3-0.7) and humid regions (AI>>1) are underrepresented in our dataset (Fig. 1b). Overall, 74% of observations fall within water-limited environments (AI≤1). Importantly, flat-gradient, water-limited conditions (C1; most susceptible) are most frequent within 1 km of the coastline, where they account for 28% of observations, but they also occur farther inland (Fig. 1c). In Fig. 1d, C1 forms contiguous coastal belts in regions such as the southeastern U.S. (ENA), Gulf of Mexico (CNA and SCA), and northeast Australia (parts of CAU and NAU). Steep-gradient, water-limited conditions (C2) dominate across all coastal distances (Fig. 1c). Near the coast, C2 accounts for 52% of observations. By contrast, susceptibility conditions, where gradients are flat but recharge is not limiting (C3), are least common.

Prevalence of trends and sensitivity to record length

Changes in GWLs alter freshwater heads and, therefore, the land-sea hydraulic gradients. For the 34-year period 1990–2024 studied, our trend analyses show that 28% of observations exhibit statistically significant GWL changes exceeding ±0.1 m yr^{-1} over 9-year windows. 21% of observations exhibit such trends when evaluated over 19-year windows. The frequency of upward and downward changes in GWLs is balanced across both periods, with a slight bias toward declines in the shorter timeframe (42% upward compared to 58% downward among absolute trends). To evaluate how strongly record length affects inferred trends, we compared slopes from overlapping 9- and 19-year windows for the subset of observations with both time frames available (Supplementary Material B-2; B-3). These are moderately correlated across windows (Spearman $\rho s = 0.58$). Trend direction is consistent in most observations (76%), while ~19% are ambiguous. Here, the 9- and 19-year slopes have opposite signs, but at least one slope is near zero ($|slope| < 0.1$ m yr^{-1}), so the apparent sign switch mainly reflects near-stable conditions in one window rather than a clear reversal. Only ~5% show clearly inconsistent opposite-sign trends with $|slope| \geq 0.1$ m yr^{-1} in both time windows. Agreement is similar at the scale of IPCC regions ($\rho s = 0.58$; 78% consistent), although a small number of regions exhibit sign changes in median trends (notably EAU, as well as NCA, SAS, and MDG in Fig. 2). Large trend magnitudes (i.e., strongly upward or strongly downward trends, $|slope| > 0.5$ m yr^{-1}) occur less

frequently over 19-year windows than over 9-year windows. This is consistent with longer records integrating low-frequency variability and episodic events (Baulon et al., 2022; Kuss and Gurdak, 2014).

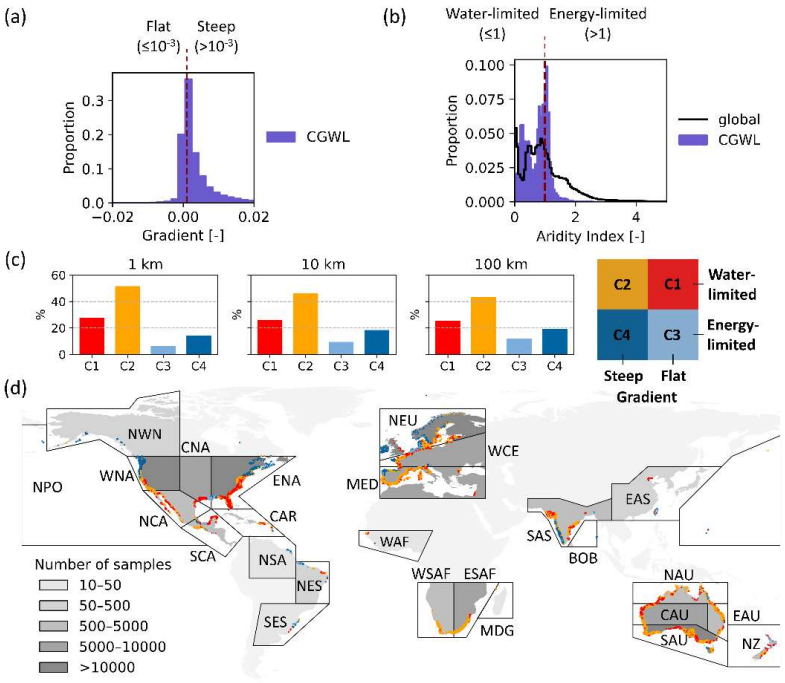

Fig. 1 Global patterns of hydroclimatic conditions indicating susceptibility of coastal groundwater systems to seawater intrusion. (a) Distribution of land-sea hydraulic gradients derived from the CGWL dataset, with a red dashed line marking the threshold separating "flat" ($\leq 10^{-3}$; landward or near-zero seaward gradients) from "steep" seaward gradients. (b) Distribution of aridity index (AI) values (Zomer et al., 2022) for the CGWL dataset and coastal regions globally, with a red dashed line marking the climatic threshold (AI~1) used to distinguish water- and energy-limited regimes. (c) Proportions of four hydroclimatic susceptibility clusters (C1–C4) at three distances from the coastline (1 km, 10 km, 100 km). (d) Global distribution of categorized observations (plotted in grid cell centers with random overlap of clusters), shown together with the number of samples in IPCC reference regions (Iturbide et al., 2020) with ≥10 observations.

For subsequent analyses, we use a combined trend product, assigning 19-year trends where available and otherwise using 9-year trends. Globally, 24% of observations show significant GWL trends, of which 54% are downward. GWL changes are mapped with their magnitude and direction in Fig. 2. The prevalence of declining and rising GWLs varies spatially, ranging from under 10% (e.g., northern Europe – NEU) to over 40% (e.g., South Africa – WSAF and ESAF; North and Central America – WNA, CAN, and NCA). Individual observations reveal strong within-region variability, with localized clusters of opposing trend directions and magnitudes.

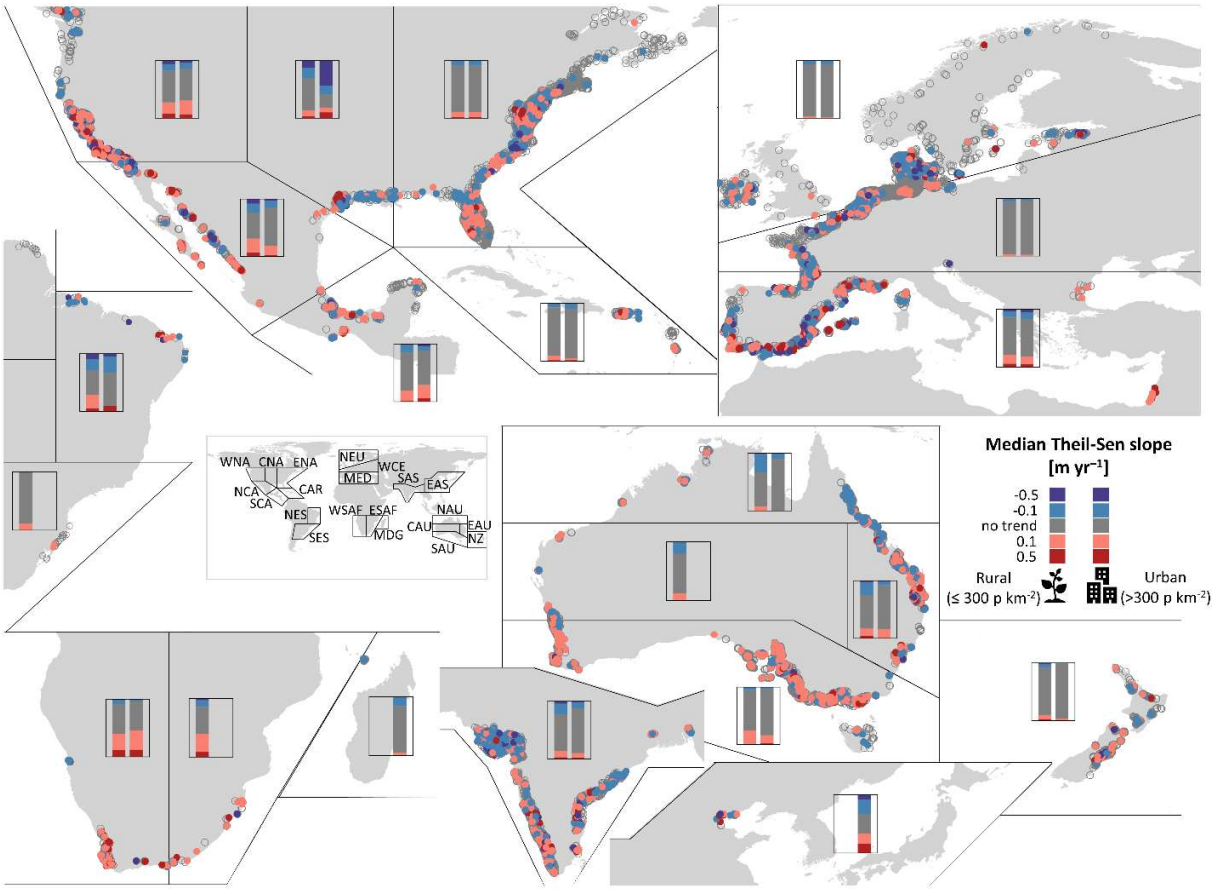

Fig. 2 Spatial patterns of recent groundwater level trends across global coastal zones, grouped by IPCC regions (Iturbide et al., 2020). Colored points on maps represent individual observations that are plotted in grid cell centers with random overlap of Theil-Sen slope trend categories on top of "no trend": strong decline (<-0.5 m year^{-1}, dark blue), moderate decline (-0.5 to -0.1 m year^{-1}, light blue), no trend (-0.1 to 0.1 m year^{-1} and/or non-significant, gray), moderate rise (0.1 to 0.5 m year^{-1}, light red), and strong rise (> 0.5 m year^{-1}, dark red). Bar charts show the proportions of trend categories per region (≥10 observations), stratified by rural (≤300 people km^{-2}) and urban (>300 people km^{-2}) areas (CIESIN, 2018). Supporting regional trend results are provided in Supplementary Material B-5.

Trends in rural and urban coastal regions

Urban and rural areas often differ in land use and water management, which can influence groundwater dynamics. We therefore stratify the dataset by a rural-urban typology (Eurostat, 2021). Fig. 2 reveals rural-urban differences in GWL changes. Overall, rural areas show a slightly higher prevalence of significant GWL trends (|slope| ≥ 0.1 m yr^{-1}) than urban areas, and the trend magnitude is weakly negatively correlated with population density (ρs: -0.17). This global rural-urban contrast is driven mainly by specific regions, including India (SAS), northern Central America (NCA), Australia (SAU, EAU, and NAU), and New Zealand (NZ). Urban observations show more frequent trends in fewer regions, especially southern Central America (SCA), central North America around the Gulf of Mexico (CAN), and eastern South Africa

(WSAF). Overall, these regional differences sum to a higher global prevalence of significant trends in rural than urban areas (26% vs 22%), with declines accounting for ~54% and ~55% of observations with trends, respectively.

Identifying hotspots of seawater intrusion susceptibility

To link hydroclimatic susceptibility from aridity and land-sea hydraulic gradients (clusters C1-C4) with dynamic change, we examine how GWL trends vary across clusters and coastal distances. First, we quantify pairwise relationships using Spearman correlations between absolute trend magnitude (|slope|) and aridity, WTD, and hydraulic gradient. These correlations are stronger inland than near the coast. At 100 km from the coastline, the trend magnitude correlates with drier conditions (ρs=0.56), with deeper water tables (ρs=0.63), and with larger land-sea hydraulic gradients (ρs=0.36). Aridity and WTD co-vary (ρs=0.50), indicating that drier conditions tend to coincide with deeper water tables. At 1 km from the coast, associations weaken but remain detectable for aridity and WTD (ρs=0.19 and ρs=0.41), whereas the association with hydraulic gradient is negligible. Second, consistent with these pairwise patterns, trend frequencies differ across susceptibility clusters (Fig. 3). Water-limited clusters (C1 and C2), which often coincide with deeper water tables in arid regions, show the highest frequencies of both upward and downward trends across all coastal distances (absolute trends: 36% and 34%). Although less susceptible in our gradient-aridity screening due to steep gradients, C2 shows the highest prevalence of GWL declines that are most pronounced further inland. Conversely, overall trend activity is much lower in energy-limited clusters (C3 and C4; 3% and 12%). Near the coast, susceptibility and change coincide most strongly: within 1 km, 28% of C1 observations show significant trends, with marginally more GWL declines than rises.

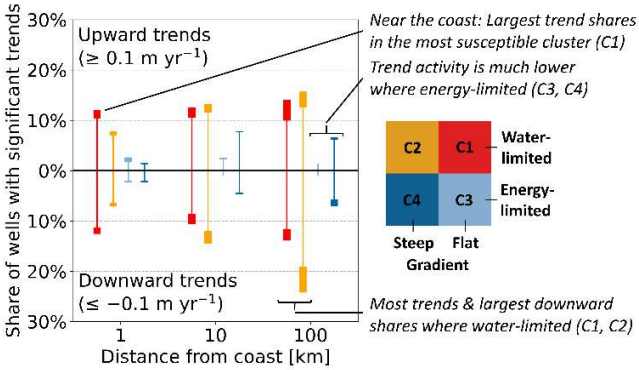

Fig. 3 Share of wells with significant upward (top, ≥0.1 m yr^{-1}) and downward (bottom, ≤-0.1 m yr^{-1}) trends as a function of distance from the coast (1, 10, 100 km). Thicker bar segments at the top and bottom indicate the shares of strongly rising (>0.5 m yr^{-1}) and strongly declining (<−0.5 m yr^{-1}) observations, respectively. Differently colored shares refer to the SWI susceptibility clusters (C1-C4).

Most trend slopes are moderate (|slope| < 0.5 m yr^{-1}), yet even modest head changes can shift land-sea gradients toward or away from flat-gradient conditions. We therefore used derived GWL trends to extrapolate whether observations may enter, remain in, or exit the flat-gradient susceptibility clusters (C1/C3) over the next decade (Fig. 4a). Persistent gradient-based hotspots (93.4% of all sites) are locations already exhibiting SWI-susceptible conditions that are projected to remain within C1 or C3 over the next decade. A smaller fraction (3.1%) is projected to stabilize, meaning they may transition out of C1/C3 if recent upward trends continue, and 3.5% are emerging hotspots, i.e., locations projected to transition into flat-gradient conditions (C1/C3) over the next decade.

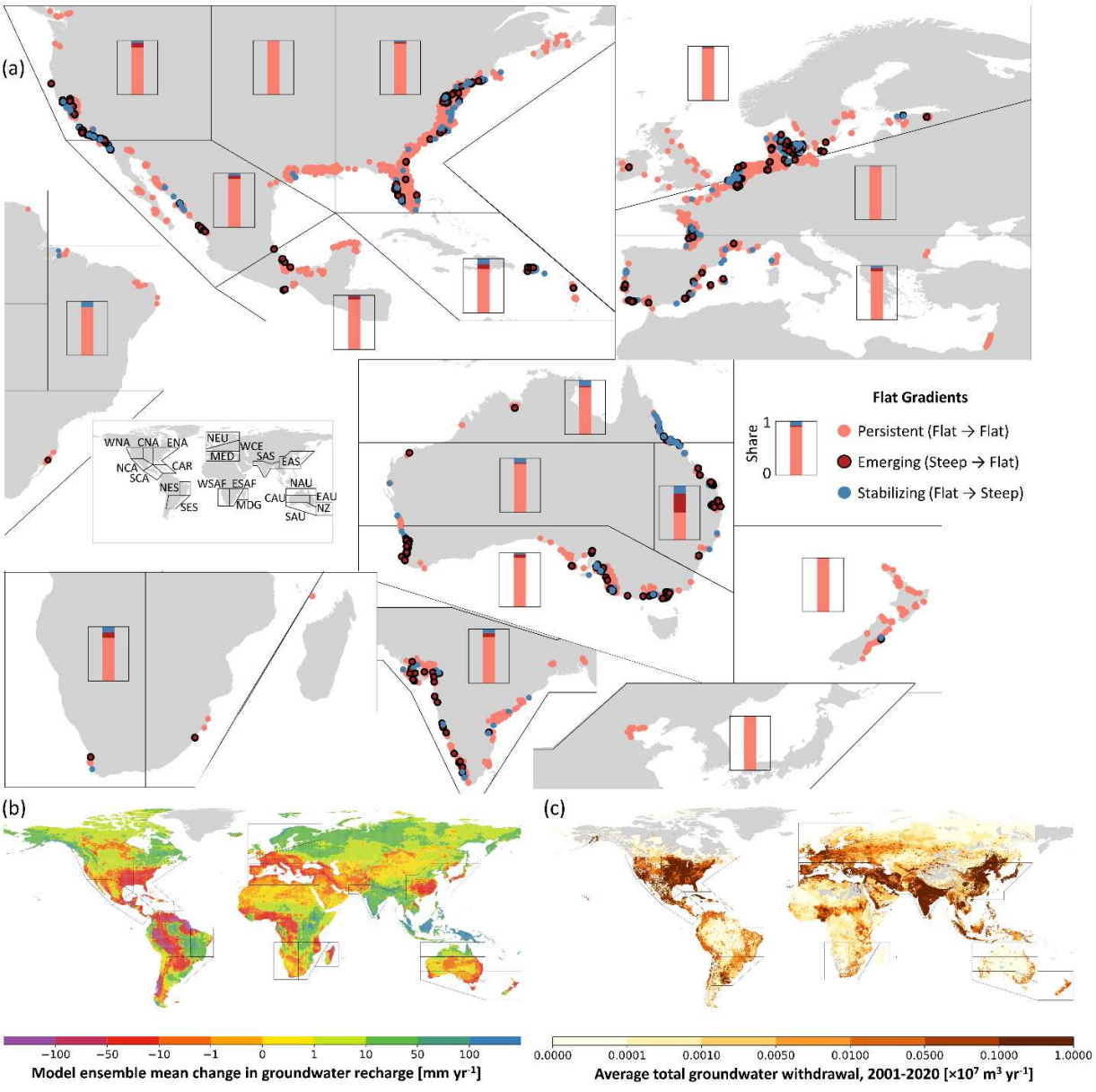

Fig. 4 (a) Spatial patterns of hydroclimatic, gradient-based SWI-susceptibility hotspots across IPCC regions (Iturbide et al., 2020), derived from trend extrapolation. Points show individual observations (grid cell centers). Hotspots are defined relative to the flat-gradient clusters C1/C3. When co-located, emerging (entering C1/C3 within 10 years) and stabilizing (exiting C1/C3 within 10 years) hotspots are randomly overlaid on persistent hotspots (in C1/C3 now and in 10 years). Bar charts show the relative proportions of hotspot types within each region (≥10 observations). (b) Model-ensemble mean change in groundwater recharge (mm yr^{-1}) between present-day warming (~1 °C) and 3 °C global warming, from the ISIMIP2b multi-model ensemble (Reinecke et al., 2021). (c) Long-term mean total groundwater withdrawal (2001–2020; $\times 10^7$ m^3 yr^{-1}), from the data-driven Global Groundwater Withdrawal (GGW) model (Nazari et al., 2025).

Discussion

The results of this study are based on deriving physically motivated indicators of SWI susceptibility from integrated in-situ GWL observations. Our hydroclimatic susceptibility framework links land-sea hydraulic gradients with aridity conditions and incorporates recent GWL changes to assess how susceptibility states may evolve, even when detailed hydrogeological information is limited. It methodologically extends elevation-based screening approaches (Jasechko et al., 2020) and complements previous large-scale GWL trend syntheses (e.g., Chávez García Silva et al., 2024; Jasechko et al., 2024) by focusing explicitly on coastal aquifer settings. In the United States, coastal regions that we classify as hydroclimatically susceptible show strong spatial concordance with areas highlighted by Jasechko et al. (2020): within 10 km of the coastline, 20% of our observations have groundwater elevations below sea level (vs 27% of wells in Jasechko et al. (2020)), and 37% have flat gradients ($\leq 10^{-3}$). Globally, our flat-gradient, water-limited cluster (C1) captures major regions with documented SWI compiled by Cao et al. (2021) and Kretschmer et al. (2025b) (Fig. 3 and Fig. 1 in the respective publications). These include the southeastern coasts of the U.S., Central America, the Mediterranean, the Cape Town area, parts of India, and southeastern Australia, which also show a higher prevalence of downward GWL trends in our analysis. Beyond these documented hotspots, our gradient-aridity framework maps the global extent and relative frequency of comparable hydroclimatic configurations, providing a quantitative screening to guide where monitoring and management could be prioritized. This also helps mitigate the urban bias noted by Kretschmer et al. (2025b) because our analysis draws on routine monitoring observations across both urban and rural settings, whereas published SWI case studies are disproportionately from urban, economically developed regions (Kretschmer et al., 2025b). At the same time, the availability of GWL observations in our analysis shows a heterogenic spatial distribution globally. Coverage is strongest in temperate regions such as Europe and the United States, whereas most of Africa, equatorial regions, large parts of South America and Asia, and many small islands remain sparsely represented or are completely missing. Accordingly, several SWI sites reported in Asia, Africa, and South America (Kretschmer et al., 2025b; Cao et al., 2021) fall outside our analyzed dataset. Our SWI susceptibility patterns therefore reflect the spatial footprint of available observations, and

the absence of mapped hotspots in data-poor regions should not be interpreted as the absence of SWI susceptibility.

This study further shows that continued GWL change can generate SWI-relevant gradients within a single decade, and that GWLs near the coastline tend to change most strongly where flat hydraulic gradients coincide with water-limited conditions (C1; most susceptible). While our observation-based indicators do not quantify volumetric freshwater losses, even small deviations and variations around the gradient threshold may become critical over longer timescales. Rising GWLs are as frequent as declines, both globally and often regionally. Coastal aquifers are therefore not uniformly moving toward greater SWI susceptibility. Instead, susceptibility can strengthen or weaken locally, and short-term variability in GWLs, even without sustained declines, can temporarily shift systems toward flat-gradient, SWI-prone conditions. This spatial and temporal variability highlights the value of sustained GWL observations for locally grounded detection of SWI-susceptible conditions.

Further increases in the marine boundary head are likely to shift additional coastlines into SWI-susceptible gradient states (Zamrsky et al., 2024; Adams et al., 2024): The global mean sea-level is currently rising at ~4.5 mm $year^{-1}$ (Hamlington et al., 2024), and is projected to rise by roughly 0.3-1.0 m by 2100 (relative to 1995–2014, depending on emissions scenario), with possible multi-meter rise on longer timescales as peak warming increases (Kopp et al., 2023). This situation can be further exacerbated by pumping-induced upconing, which can cause SWI even further inland (Jakovovic et al., 2011). This matters because our study shows that deep aquifers in rural, arid regions exhibit more widespread declines. Because these systems often respond slowly, management interventions may take years to decades to translate into measurable head recovery, so expectations for SWI susceptibility and monitoring strategies need to account for delayed results. Furthermore, the spatial distribution of significant GWL changes does not align with population density. This should be read as an observed GWL signal, not a direct proxy for local groundwater use, because urban demand is partly met by pumping outside cities. However, our results align with Jasechko et al. (2024), who found widespread declines in dryland aquifers, particularly under croplands. Hence, groundwater-dependent agricultural regions may face disproportionate SWI susceptibility where high extraction pressures coincide with limited regulatory oversight. Persistent or emerging flat-gradient patterns in our study frequently co-occur with regions where sectoral groundwater withdrawals are already high (Fig. 4c), with agriculture as the dominant groundwater user and increasing withdrawals in many regions since 2001 (Nazari et al., 2025). Beyond SWI, some regions with relatively low gradient-based susceptibility, such as parts of South Africa, show substantial GWL declines together with projected groundwater recharge reductions (Fig. 4b), indicating emerging groundwater-stress risks that are highly relevant in the context of "Day Zero" drought-driven water-scarcity crises, where prolonged hydroclimatic deficits and high demand

can push water systems into acute supply shortfalls (Ravinandrasana and Le Franzke, 2025). In such situations, groundwater can be considered a fallback supply (Nolte et al., 2021), but in coastal settings where our indicators suggest SWI susceptibility and/or declining GWLs, this option may be constrained by limited availability.

Conclusions

This study provides the first global observation-based assessment of hydroclimatic conditions associated with SWI susceptibility in coastal groundwater systems that is based on in-situ GWL observations from ~480,000 coastal monitoring locations. By combining land-sea hydraulic gradients, aridity, and recent GWL trends in a bottom-up approach that captures spatiotemporal signals often missed by static frameworks and/or coarse top-down approaches, the study delivers three main contributions. First, it translates the available monitoring footprint into globally comparable quantities that can inform large-scale assessments and reporting (e.g., by international frameworks). Second, the study maps where potentially susceptible conditions occur and where they are changing, helping prioritize monitoring and management in coastal regions where risk may be shifting in real time. Third, it provides observation-based indicators that can be systematically incorporated into SWI risk assessments and used as constraints to evaluate and improve large-scale models that simulate unmonitored coasts. At the same time, the hydroclimatic susceptibility indicators do not by themselves resolve local vulnerability or control-response relationships. Doing so requires more detailed hydrogeologic characterization, co-located salinity monitoring, and improved global datasets of key controls, alongside broader efforts to expand and strengthen groundwater observations, particularly in regions with large observational gaps. Avoiding or reducing SWI in susceptible settings is critical because salinization of groundwater threatens safe drinking-water supplies, lowers agricultural productivity, and degrades coastal and nearshore ecosystems. Looking ahead, our findings highlight that stronger monitoring and data-synthesis efforts can enable scalable, observation-based tools to detect emerging SWI risk early, improve system understanding, and inform timely adaptation. Such advances are increasingly important as projected shifts in groundwater recharge, continued sea-level rise, and anthropogenic pressures interact with existing flat-gradient settings in many coastal regions.

Methods

We used the Coastal Groundwater Level (CGWL) dataset, a newly compiled global resource of in-situ coastal GWL observations from governmental monitoring networks and public portals (Supplementary Material A). The CGWL dataset comprises ~629,000 well records (~480,000 unique locations at 3-decimal coordinates) from wells within 100 km of the coastline and with WTDs shallower than 100 m (Supplementary Material A-1). Raw groundwater data were quality controlled and harmonized to consistent

groundwater depth (WTD; ground-surface reference) and groundwater elevation, using source-provided elevations where available and otherwise CoastalDEM (Kulp and Strauss, 2019) or SRTM (NASA JPL, 2020). We aggregated groundwater information to hexagonal grid cells with a mean cell area of 0.74 km² (H3-8; Uber Technologies Inc 2024) and refer to these grid-cell aggregates as "observations".

Groundwater hydraulic gradients

Land-sea hydraulic gradients were calculated at the grid level using median groundwater elevation and the median Euclidean distance of wells in the cell to the coastline (dataset: Sayre et al., 2021). Using medians reduces sensitivity to outliers but also smooths short-term extremes in the hydraulic head that can be relevant for SWI. Because this proxy does not resolve time-varying coastal boundary heads, non-linear flow paths, or within-cell hydrogeologic heterogeneity, gradients may be biased high or low at individual locations. We therefore interpreted them as a first-order, observation-based screening diagnostic of prevailing coastal head conditions. The sample size for gradient analysis comprised 232,419 grid cells with available groundwater elevation and coastline distance data.

Trend analysis

To quantify recent GWL change, we filtered monthly CGWL time series and computed monotonic trends over 9- and 19-year windows within 1990–2024. The record lengths used for the trend analysis were chosen iteratively to balance temporal robustness against global support, consistent with prior large-scale groundwater trend studies (Jasechko et al., 2024). A detailed discussion of window-length trade-offs is provided in the Supplementary Material B-3. Time-series selection further allowed variable sampling while limiting seasonal distortion (Supplementary Material B-1). This yielded 51,263 unique monitoring locations with sufficient data to estimate a 9-year trend. Of these, 20,857 locations also met the minimum length for a 19-year trend. Where both are available, the 9-year window corresponds to the final 9 years of the 19-year window. Monotonic trends in GWLs were calculated using the non-parametric modified Mann-Kendall test (Yue and Wang, 2004), and corresponding trend magnitudes were estimated using Sen's slope (Sen, 1968). Trends were computed at the well level and subsequently aggregated to H3-8 grid cells by taking the median of slope values, regardless of individual statistical significance ($p > 0.05$); however, significance flags were retained to support additional filtering. Trend slopes were classified into five trend categories: strongly downward (<-0.5 m yr^{-1}), moderately downward (-0.5 to -0.1 m yr^{-1}), no trend (between -0.1 and 0.1 m yr^{-1} and/or non-significant), moderately upward (0.1 to 0.5 m yr^{-1}), and strongly upward (>0.5 m yr^{-1}). Only a small fraction of results classified as "no trend" are non-significant solely due to statistical insignificance (5.6% for 9-year trends and 1.7% for 19-year trends). After aggregation, trend results were available for

36,579 grid cells (9-year) and 17,703 grid cells (19-year), so that 19-year trends support ~41% of grid-level trend estimates globally (Supplementary Material B-2).

Hydroclimatic classification and hotspot extrapolation

Hydroclimatic susceptibility was applied along two axes: aridity (as a proxy for recharge limitation) and land-sea hydraulic gradient (as a proxy for the tendency toward seaward discharge versus inland salinity advance). To classify gradients, we used two categories based on model-informed thresholds: flat ($\leq 10^{-3}$, landward or near-zero seaward gradients) and steep seaward gradients ($>10^{-3}$), following Ferguson and Gleeson (2012) and Kretschmer et al. (2025a), who showed that gradients lower than 10^{-3} are more prone to SWI or to the persistence of saline groundwater. Each H3-8 grid cell was further assigned the aridity index (AI) from Zomer et al. (2022), which represents the ratio of precipitation to potential evapotranspiration. Cells were categorized as either water-limited (AI≤1) or energy-limited (AI>1). These binary classes define clusters C1-C4 used throughout this study:

- C1 (most susceptible): Flat gradient ($\leq 10^{-3}$) & water-limited (AI≤1)
- C2: Steep gradient ($>10^{-3}$) & water-limited (AI≤1)
- C3: Flat gradient ($\leq 10^{-3}$) & energy-limited (AI>1)
- C4 (least susceptible): Steep gradient ($>10^{-3}$) & energy-limited (AI>1)

To analyze potential hotspot persistence/emergence under continued change, we extrapolated groundwater elevation using the estimated trend slope over a 10-year horizon, recomputed the projected gradient, and evaluated whether grid cells would remain in, enter, or exit flat-gradient conditions (C1/C3). This provides a straightforward diagnostic that does not account for potential nonlinearities in drivers of GWL trends or management responses.

Preparing secondary datasets for contextual analyses

The global aridity index (Zomer et al., 2022) is used directly in the SWI susceptibility classification. All other secondary datasets were compiled only to contextualize and interpret gradients and GWL trends. Specifically, Fig. 4b-c shows gridded sectoral groundwater withdrawals (Nazari et al., 2025) and a multi-model ensemble of groundwater recharge change (Reinecke et al., 2021) for visual comparison with our results. We prepared the population density of the year 2020 (CIESIN, 2018) to derive rural-urban classes following Eurostat (2021). This dataset was preprocessed in ArcGIS Pro where information was derived for H3-8 grid cells using zonal statistics.

Limitations

- **Spatial aggregation framework:** We adopted the regular, globally near-equal-area H3-8 grid (Uber Technologies Inc, 2024) as a transparent, assumption-light spatial unit that provides area-representative summaries while reducing the mixing of heterogeneous aquifer conditions relative to coarser aggregation units. This choice reflects that, at the global scale, aquifer boundaries and vertical structure cannot be delineated consistently from the available data in the CGWL dataset and existing global hydrogeologic datasets (Supplementary Material A-2). We used H3-8 grid cells as the primary analysis unit, but repeated all key diagnostics on coastal HydroBASINS level-12 catchments (HYBAS-12; Lehner and Grill, 2013) as a sensitivity test. Aggregation error, quantified as the RMSE between well-level and unit-level median WTD, is lowest for H3-8 and increases for larger aggregation units, while it decreases primarily with the number of wells per unit. HYBAS-12 basins are on average ~141 km² (about four times larger than H3-6 hexagonal grid cells, ~36 km²), yet the share of multi-well units is similar for HYBAS-12 and H3-6, and aggregation error is slightly larger for HYBAS-12, indicating no systematic reduction of aggregation error relative to grid-based schemes with comparable well support (Supplementary Material A-3). We therefore assume that any discrepancies between H3-8 and HYBAS-12 primarily reflect aggregation and sampling effects, that is, how differently sized spatial units mix heterogeneous conditions and how unevenly well density weights regional summaries. Against this background, HYBAS-12 closely reproduces the H3-8 patterns across IPCC coastal regions and distance-to-coast bands for flat-gradient prevalence, trend activity ($|\text{slope}| \geq 0.1$ m yr^{-1}), the fraction of downward trends among trend-active units, and the share of persistent/emerging flat-gradient hotspots (Spearman $\rho s = 0.87–0.95$). Global differences are small, although a few regions deviate by >10 percentage points; for example, grids yield higher flat-gradient prevalence in Western Europe (WCE), while HYBAS-12 shifts the Caribbean (CAR) toward more upward and fewer downward trends, resulting in fewer persistent/emerging hotspots (Supplementary Material B-4).
- **Bottom-up approach and representativeness limits:** Our analysis is global in extent but bottom-up, scaling local well observations to consistent spatial units, and from there to regional and global SWI susceptibility indicators. The spatial representativeness of these indicators, both geographically and with respect to hydrogeologic settings, is constrained by uneven data coverage globally and the limited hydrogeologic characterization (notably aquifer system architecture and confinement). Our chosen fine grid-based aggregation can overweight densely monitored coastal areas and may regionally yield slightly different hotspot and trend-activity shares than coarser units, but it reduces the mixing of heterogeneous aquifer conditions.
- **Simplifications with GWL-based indicators:** While this study uses GWL-based indicators to assess SWI susceptibility, it necessarily simplifies the physical complexity of coastal aquifer systems, where salinization can propagate through multiple interconnected pathways: over land (storm surge and tidal flooding), under land via groundwater transport, and through natural and engineered surface-water networks, and via vertical

processes such as upconing of deeper saline water beneath pumping wells (Helton et al., 2025; Werner et al., 2012). Our indicators do not explicitly represent salinity or density-driven flow, limited by salinity observations being far less available than GWL time series at large scales (Panthi et al., 2022; Thorslund and van Vliet, 2020) and co-located water-quality and water-quantity records being uncommon (Ebeling et al., 2022). The indicators also simplify temporal dynamics relevant to SWI. In particular, gradients often rely on a single or short snapshot of head data, which is insufficient to quantify variability or detect shifts, while monotonic trends summarize net change over the analysis window and may miss transient or nonlinear changes.

- **Trend robustness and record-length sensitivity:** Since trend direction at individual locations can be sensitive to record length and to the timing of multiannual variability or management interventions, regions with spatio-temporally inconsistent trends require particularly careful interpretation. However, our 9- vs 19-year comparison indicates that, while longer records are generally more robust, 9-year time series already capture the qualitative direction of GWL change for most regions, with notable exceptions such as in southeastern Australia and India, where declines are stronger and more frequent in the more recent 9-year window. Multi-window trend reporting can serve as a practical robustness check when long GWL records are unavailable.

- **Limits to causal inference and attribution:** In general, this study does not establish causation. Because gridded population products redistribute census counts, population-based contrasts (and any future projections) carry spatially heterogeneous uncertainty. Specifically, they can systematically underrepresent rural populations and misallocate density within cities (Láng-Ritter et al., 2025; Kuffer et al., 2022). Given the substantial uncertainties in both global recharge projections and pumping estimates when interpreted at the scale of local observations (Reinecke et al., 2021; Nazari et al., 2025), we do not directly attribute the observed gradients and trends to these drivers (Fig. 4b-c). Instead, we use the aridity index as a proxy for recharge limitation and, indirectly, for potential future increases in water stress and demand. However, we acknowledge that its bi-categorical application (like the gradient split) is a coarse simplification that facilitates transparent global screening, but can mask precipitation effects relevant to recharge and compress diverse hydro-climatic (and hydro-ecological) settings into broad classes (Taylor et al., 2013; Zomer et al., 2022).

Acknowledgments

The authors would like to thank all of the governmental agencies listed in Supplementary Material A that supported this work by providing groundwater data and being available to answer questions about the data.

This work was financed within the framework of the Helmholtz Institute for Climate Service Science (HICSS), a cooperation between the Climate Service Center Germany (GERICS) and Universität Hamburg, Germany, and conducted as part of the Future-H2O (Future climate and land-use change impacts on groundwater recharge rates and water quality for water resources) project.

CRediT authorship contribution statement

A. Nolte: Conceptualization, Data curation, Formal analysis, Investigation, Methodology, Writing – original draft, Writing – review & editing. **S. Bender:** Funding acquisition, Supervision, Writing – review & editing. **J. Hartmann:** Funding acquisition, Supervision, Writing – review & editing. **S. Baltruschat:** Methodology, Writing – review & editing. **N. Moosdorf:** Methodology, Writing – review & editing. **R. Reinecke:** Conceptualization, Formal analysis, Methodology, Writing – original draft, Writing – review & editing

Data availability statement

The CGWL dataset is publicly available on Zenodo under a CC-BY-NC license, including all data sources obtained with permission for publishing or under open licenses: [link will be provided in peer-reviewed manuscript]. Code and data for conducting trend and SWI susceptibility analyses are also available on Zenodo: [link will be provided in peer-reviewed manuscript]. Additional datasets used in these analyses are referenced within the same repository.

References

Adams, K. H., Reager, J. T., Buzzanga, B. A., David, C. H., Sawyer, A. H., and Hamlington, B. D.: Climate-induced saltwater intrusion in 2100: Recharge-driven severity, sea level-driven prevalence, Geophysical Research Letters, 51, e2024GL110359, doi:10.1029/2024GL110359, 2024.

Arifin, A., Shamsudduha, M., am Ramdhan, Rateb, A., Scanlon, B. R., Setiawan, T., Iman, M. I., Husna, A., and Taylor, R. G.: Plausibility criteria for GRACE-derived groundwater storage changes from aquifers globally, Geophysical Research Letters, 52, e2025GL118580, doi:10.1029/2025GL118580, 2025.

Baulon, L., Allier, D., Massei, N., Bessiere, H., Fournier, M., and Bault, V.: Influence of low-frequency variability on groundwater level trends, Journal of Hydrology, 606, 127436, doi:10.1016/j.jhydrol.2022.127436, 2022.

Berghuijs, W. R., Collenteur, R. A., Jasechko, S., Jaramillo, F., Luijendijk, E., Moeck, C., van der Velde, Y., and Allen, S. T.: Groundwater recharge is sensitive to changing long-term aridity, Nature Climate Change, 14, 357–363, doi:10.1038/s41558-024-01953-z, 2024.

Cao, T., Han, D., and Song, X.: Past, present, and future of global seawater intrusion research: A bibliometric analysis, Journal of Hydrology, 603, 126844, doi:10.1016/j.jhydrol.2021.126844, 2021.

Chávez García Silva, R., Reinecke, R., Copty, N. K., Barry, D. A., Heggy, E., Labat, D., Roggero, P. P., Borchardt, D., Rode, M., and Gómez-Hernández, J. J.: Multi-decadal groundwater observations reveal surprisingly stable levels in southwestern Europe, Communications Earth & Environment, 5, 387, doi:10.1038/s43247-024-01554-w, 2024.

CIESIN: Gridded Population of the World, Version 4 (GPWv4): Population Density, Revision 11, NASA Socioeconomic Data and Applications Center (SEDAC) [data set], doi:10.7927/H49C6VHW, 2018.

Cosby, A. G., Lebakula, V., Smith, C. N., Wanik, D. W., Bergene, K., an Rose, Swanson, D., and de Bloom: Accelerating growth of human coastal populations at the global and continent levels: 2000–2018, Scientific Reports, 14, 22489, doi:10.1038/s41598-024-73287-x, 2024.

Costall, A. R., Harris, B. D., Teo, B., Schaa, R., Wagner, F. M., and Pigois, J. P.: Groundwater throughflow and seawater intrusion in high quality coastal aquifers, Scientific Reports, 10, 9866, doi:10.1038/s41598-020-66516-6, 2020.

Costantini, M., Colin, J., and Decharme, B.: Projected climate-driven changes of water table depth in the world's major groundwater basins, Earth's Future, 11, e2022EF003068, doi:10.1029/2022EF003068, 2023.

Cuthbert, M. O., Gleeson, T., Moosdorf, N., Befus, K. M., Schneider, A., Hartmann, J., and Lehner, B.: Global patterns and dynamics of climate–groundwater interactions, Nature Climate Change, 9, 137–141, doi:10.1038/s41558-018-0386-4, 2019.

Dyring, M., Hofmann, H., Stanton, D., Moss, P., and Froend, R.: Ecohydrology of coastal aquifers in humid environments and implications of a drying climate, Ecohydrology, 16, e2491, doi:10.1002/eco.2491, 2022.

Ebeling, P., Kumar, R., Lutz, S. R., Nguyen, T., Sarrazin, F., Weber, M., Büttner, O., Attinger, S., and Musolff, A.: Water quality, discharge and catchment attributes for large-sample studies in Germany – QUADICA, Earth System Science Data, 14, 3715–3741, doi:10.5194/essd-2022-6, 2022.

Eurostat: Applying the Degree of Urbanisation: A methodological manual to define cities, towns and rural areas for international comparisons, Publications Office of the European Union, Luxembourg, 2021.

Famiglietti, J. S. and Rodell, M.: Water in the balance, Science, 340, 1300–1301, doi:10.1126/science.1240843, 2013.

Fan, Y., Li, H., and Miguez-Macho, G.: Global patterns of groundwater table depth, Science, 339, 940–943, doi:10.1126/science.1229881, 2013.

Fan, Y., Li, H., and Miguez-Macho, G.: Global patterns of groundwater table depth [data set]., http://thredds-gfnl.usc.es/thredds/catalog/GLOBALWTDFTP/catalog.html, last access: 08 March 2023, 2023.

Ferguson, G. and Gleeson, T.: Vulnerability of coastal aquifers to groundwater use and climate change, Nature Climate Change, 2, 342–345, doi:10.1038/nclimate1413, 2012.

519 Frappart, F. and Ramillien, G.: Monitoring groundwater storage changes using the Gravity
520 Recovery and Climate Experiment (GRACE) satellite mission: A review, Remote Sensing,
521 10, 829, doi:10.3390/rs10060829, 2018.

522 Ghirardelli, A., Straffelini, E., Park, E., D'Agostino, V., Masin, R., and Tarolli, P.: Global impact
523 of seawater intrusion on coastal agriculture, Environmental Research Letters, 20, 13005,
524 doi:10.1088/1748-9326/ad9bcd, 2024.

525 Gleeson, T., Cuthbert, M., Ferguson, G., and Perrone, D.: Global groundwater sustainability,
526 resources, and systems in the Anthropocene, Annual Review of Earth and Planetary Sciences,
527 48, 431–463, doi:10.1146/annurev-earth-071719-055251, 2020.

528 Gleeson, T., Wagener, T., Döll, P., Zipper, S. C., West, C., Wada, Y., Taylor, R., Scanlon, B.,
529 Rosolem, R., Rahman, S., Oshinlaja, N., Maxwell, R., Lo, M.-H., Kim, H., Hill, M.,
530 Hartmann, A., Fogg, G., Famiglietti, J. S., Ducharne, A., Graaf, I. de, Cuthbert, M., Condon,
531 L., Bresciani, E., and Bierkens, M. F. P.: GMD perspective: The quest to improve the
532 evaluation of groundwater representation in continental- to global-scale models, Geoscientific
533 Model Development, 14, 7545–7571, doi:10.5194/gmd-14-7545-2021, 2021.

534 Hamlington, B. D., Bellas-Manley, A., Willis, J. K., Fournier, S., Vinogradova, N., Nerem, R. S.,
535 Piecuch, C. G., Thompson, P. R., and Kopp, R.: The rate of global sea level rise doubled
536 during the past three decades, Communications Earth & Environment, 5, 601,
537 doi:10.1038/s43247-024-01761-5, 2024.

538 Helton, A. M., Dennedy-Frank, P. J., Emanuel, R. E., Neubauer, S. C., Adams, K. H., Ardon, M.,
539 Band, L., Befus, K. M., Borstlap, H., and Duberstein, J. A.: Over, under, and through:
540 Hydrologic connectivity and the future of coastal landscape salinization, Water Resources
541 Research, 61, e2024WR038720, doi:10.1029/2024WR038720, 2025.

542 IPCC: Climate change 2021: The Physical Science Basis: Contribution of Working Group I to the
543 Sixth Assessment Report of the Intergovernmental Panel on Climate Change, Cambridge
544 University Press, Cambridge, United Kingdom and New York, NY, USA, 2021.

545 Iturbide, M., Gutiérrez, J. M., Alves, L. M., Bedia, J., Cerezo-Mota, R., Cimadevilla, E., Cofiño,
546 A. S., Di Luca, A., Faria, S. H., Gorodetskaya, I. V., Hauser, M., Herrera, S., Hennessy, K.,
547 Hewitt, H. T., Jones, R. G., Krakovska, S., Manzanas, R., Martínez-Castro, D., Narisma, G.
548 T., Nurhati, I. S., Pinto, I., Seneviratne, S. I., van den Hurk, B., and Vera, C. S.: An update of
549 IPCC climate reference regions for subcontinental analysis of climate model data: definition
550 and aggregated datasets, Earth System Science Data, 12, 2959–2970, doi:10.5194/essd-12-
551 2959-2020, 2020.

552 Jakovovic, D., Werner, A. D., and Simmons, C. T.: Numerical modelling of saltwater up-coning:
553 comparison with experimental laboratory observations, Journal of Hydrology, 402, 261–273,
554 doi:10.1016/j.jhydrol.2011.03.021, 2011.

555 Jasechko, S., Perrone, D., Seybold, H., Fan, Y., and Kirchner, J. W.: Groundwater level
556 observations in 250,000 coastal US wells reveal scope of potential seawater intrusion, Nature
557 Communications, 11, 3229, doi:10.1038/s41467-020-17038-2, 2020.

558 Jasechko, S., Seybold, H., Perrone, D., Fan, Y., Shamsudduha, M., Taylor, R. G., Fallatah, O.,
559 and Kirchner, J. W.: Rapid groundwater decline and some cases of recovery in aquifers
560 globally, Nature, 625, 715–721, doi:10.1038/s41586-023-06879-8, 2024.

Kopp, R. E., Oppenheimer, M., O'Reilly, J. L., Drijfhout, S. S., Edwards, T. L., Fox-Kemper, B., Garner, G. G., Golledge, N. R., Hermans, T. H. J., and Hewitt, H. T.: Communicating future sea-level rise uncertainty and ambiguity to assessment users, Nature Climate Change, 13, 648–660, doi:10.1038/s41558-023-01691-8, 2023.

Kretschmer, D. V., Michael, H., Moosdorf, N., Essink, G. O., Bierkens, M. F. P., Wagener, T., and Reinecke, R.: Controls on coastal saline groundwater across North America, Environmental Research Letters, 20, 24065, doi:10.1088/1748-9326/ada973, 2025a.

Kretschmer, D. V., Michael, H. A., Moosdorf, N., Oude Essink, G. H. P., Bierkens, M. F. P., Wagener, T., and Reinecke, R.: A perceptual model of drivers and limiters of coastal groundwater dynamics, Hydrological Processes, 39, e70058, doi:10.1002/hyp.70058, 2025b.

Kuffer, M., Owusu, M., Oliveira, L., Sliuzas, R., and van Rijn, F.: The missing millions in maps: Exploring causes of uncertainties in global gridded population datasets, ISPRS International Journal of Geo-Information, 11, 403, 2022.

Kulp, S. A. and Strauss, B. H.: New elevation data triple estimates of global vulnerability to sea-level rise and coastal flooding, Nature Communications, 10, 4844, doi:10.1038/s41467-019-12808-z, 2019.

Kuss, A. J. M. and Gurdak, J. J.: Groundwater level response in US principal aquifers to ENSO, NAO, PDO, and AMO, Journal of Hydrology, 519, 1939–1952, doi:10.1016/j.jhydrol.2014.09.069, 2014.

Lall, U., Josset, L., and Russo, T.: A Snapshot of the World's Groundwater Challenges, Annual Review of Environment and Resources, 45, 171–194, doi:10.1146/annurev-environ-102017-025800, 2020.

Láng-Ritter, J., Keskinen, M., and Tenkanen, H.: Global gridded population datasets systematically underrepresent rural population, Nature Communications, 16, 2170, doi:10.1038/s41467-025-56906-7, 2025.

Lecher, A. L. and Mackey, K. R. M.: Synthesizing the effects of submarine groundwater discharge on marine biota, Hydrology, 5, 60, doi:10.3390/hydrology5040060, 2018.

Lehner, B. and Grill, G.: Global river hydrography and network routing: baseline data and new approaches to study the world's large river systems, Hydrological Processes, 27, 2171–2186, doi:10.1002/hyp.9740, 2013.

Luijendijk, E., Gleeson, T., and Moosdorf, N.: Fresh groundwater discharge insignificant for the world's oceans but important for coastal ecosystems, Nature Communications, 11, 1260, doi:10.1038/s41467-020-15064-8, 2020.

Ma, Y., Leonarduzzi, E., Defnet, A., Melchior, P., Condon, L. E., and Maxwell, R. M.: Water table depth estimates over the contiguous united states using a random forest model, Groundwater, 62, 34–43, 2024.

Michael, H. A., Russoniello, C. J., and Byron, L. A.: Global assessment of vulnerability to sea-level rise in topography-limited and recharge-limited coastal groundwater systems, Water Resources Research, 49, 2228–2240, doi:10.1002/wrcr.20213, 2013.

600 Morgan, L. K. and Werner, A. D.: A national inventory of seawater intrusion vulnerability for
601 Australia, Journal of Hydrology: Regional Studies, 4, 686–698,
602 doi:10.1016/j.ejrh.2015.10.005, 2015.

603 Mueller, W., Zamrsky, D., Essink, G. O., Fleming, L. E., Deshpande, A., Makris, K. C., Wheeler,
604 B. W., Newton, J. N., Narayan, K. V., and Naser, A. M.: Saltwater intrusion and human
605 health risks for coastal populations under 2050 climate scenarios, Scientific Reports, 14,
606 15881, 2024.

607 NASA JPL: NASADEM Merged DEM Global 1 arc second V001 [data set], NASA Land
608 Processes Distributed Active Archive Center,
609 doi:10.5067/MEASURES/NASADEM/NASADEM_HGT.001, 2020.

610 Nazari, S., Reinecke, R., and Moosdorf, N.: Global estimates of groundwater withdrawal trends
611 and uncertainties, Environmental Research Letters, 20, 94043, doi:10.1088/1748-
612 9326/adf6ca, 2025.

613 Neumann, B., Vafeidis, A. T., Zimmermann, J., and Nicholls, R. J.: Future coastal population
614 growth and exposure to sea-level rise and coastal flooding-a global assessment, PloS one, 10,
615 e0118571, doi:10.1371/journal.pone.0118571, 2015.

616 Nolte, A., Eley, M., Schöniger, M., Gwapedza, D., Tanner, J., Mantel, S. K., and Scheihing, K.:
617 Hydrological modelling for assessing spatio-temporal groundwater recharge variations in the
618 water-stressed Amathole Water Supply System, Eastern Cape, South Africa, Hydrological
619 Processes, 35, e14264, doi:10.1002/hyp.14264, 2021.

620 Nolte, A., Haaf, E., Heudorfer, B., Bender, S., and Hartmann, J.: Disentangling coastal
621 groundwater level dynamics in a global dataset, Hydrology and Earth System Sciences, 28,
622 1215–1249, doi:10.5194/hess-28-1215-2024, 2024.

623 Panthi, J., Pradhanang, S. M., Nolte, A., and Boving, T. B.: Saltwater intrusion into coastal
624 aquifers in the contiguous United States - A systematic review of investigation approaches
625 and monitoring networks, Science of the Total Environment, 836, 155641,
626 doi:10.1016/j.scitotenv.2022.155641, 2022.

627 Ravinandrasana, V. P. and Le Franzke, C.: The first emergence of unprecedented global water
628 scarcity in the Anthropocene, Nature Communications, 16, 8281, doi:10.1038/s41467-025-
629 63784-6, 2025.

630 Reinecke, R., Gnann, S., Stein, L., Bierkens, M., Graaf, I. de, Gleeson, T., Essink, G. O.,
631 Sutanudjaja, E. H., Vargas, C. R., and Verkaik, J.: Uncertainty in model estimates of global
632 groundwater depth, Environmental Research Letters, 19, 114066, doi:10.1088/1748-
633 9326/ad8587, 2024.

634 Reinecke, R., Müller Schmied, H., Trautmann, T., Andersen, L. S., Burek, P., Flörke, M.,
635 Gosling, S. N., Grillakis, M., Hanasaki, N., and Koutroulis, A.: Uncertainty of simulated
636 groundwater recharge at different global warming levels: a global-scale multi-model
637 ensemble study, Hydrol. Earth Syst. Sci., 25, 787–810, 2021.

638 Richardson, C. M., Davis, K. L., Ruiz-González, C., Guimond, J. A., Michael, H. A., Paldor, A.,
639 Moosdorf, N., and Paytan, A.: The impacts of climate change on coastal groundwater, Nature
640 Reviews Earth & Environment, 5, 100–119, doi:10.1038/s43017-023-00500-2, 2024.

Sayre, R., Butler, K., van Graafeiland, K., Breyer, S., Wright, D., Frye, C., Karagulle, D., Martin, M., Cress, J., Allen, T., Allee, R., Parsons, R., Nyberg, B., Costello, M., Harris, P., and Muller-Karger, F.: A global ecological classification of coastal segment units to complement marine biodiversity observation network assessments, Oceanography, 34, 120–129, doi:10.5670/oceanog.2021.219, 2021.

Sen, P. K.: Estimates of the regression coefficient based on Kendall's tau, Journal of the American statistical association, 63, 1379–1389, 1968.

Shokri-Kuehni, S. M. S., Raaijmakers, B., Kurz, T., Or, D., Helmig, R., and Shokri, N.: Water table depth and soil salinization: From pore-scale processes to field-scale responses, Water Resources Research, 56, e2019WR026707, doi:10.1029/2019WR026707, 2020.

Spinoni, J., Barbosa, P., Cherlet, M., Forzieri, G., McCormick, N., Naumann, G., Vogt, J. V., and Dosio, A.: How will the progressive global increase of arid areas affect population and land-use in the 21st century?, Global and Planetary Change, 205, 103597, doi:10.1016/j.gloplacha.2021.103597, 2021.

Taylor, R. G., Scanlon, B., Döll, P., Rodell, M., van Beek, R., Wada, Y., Longuevergne, L., Leblanc, M., Famiglietti, J. S., and Edmunds, M.: Ground water and climate change, Nature Climate Change, 3, 322–329, doi:10.1038/nclimate1744, 2013.

Thorslund, J. and van Vliet, M. T. H.: A global dataset of surface water and groundwater salinity measurements from 1980-2019, Scientific Data, 7, 231, doi:10.1038/s41597-020-0562-z, 2020.

Tully, K., Gedan, K., Epanchin-Niell, R., Strong, A., Bernhardt, E. S., BenDor, T., Mitchell, M., Kominoski, J., Jordan, T. E., and Neubauer, S. C.: The invisible flood: The chemistry, ecology, and social implications of coastal saltwater intrusion, BioScience, 69, 368–378, doi:10.1093/biosci/biz027, 2019.

Uber Technologies Inc: H3: Hexagonal hierarchical geospatial indexing system [software], https://h3geo.org/, 2024.

United Nations: The United Nations World Water Development Report 2022: Groundwater - Making the invisible visible, doi:10.18356/9789210015363, 2022.

Venâncio, C., Ribeiro, R., and Lopes, I.: Seawater intrusion: An appraisal of taxa at most risk and safe salinity levels, Biological Reviews, 97, 361–382, doi:10.1111/brv.12803, 2022.

Werner, A. D.: On the classification of seawater intrusion, Journal of Hydrology, 551, 619–631, doi:10.1016/j.jhydrol.2016.12.012, 2017.

Werner, A. D., Ward, J. D., Morgan, L. K., Simmons, C. T., Robinson, N. I., and Teubner, M. D.: Vulnerability indicators of sea water intrusion, Groundwater, 50, 48–58, doi:10.1111/j.1745-6584.2011.00817.x, 2012.

Yue, S. and Wang, C.: The Mann-Kendall test modified by effective sample size to detect trend in serially correlated hydrological series, Water Resources Management, 18, 201–218, doi:10.1023/B:WARM.0000043140.61082.60, 2004.

Zamrsky, D., Oude Essink, G. H. P., and Bierkens, M. F. P.: Global impact of sea level rise on coastal fresh groundwater resources, Earth's Future, 12, e2023EF003581, doi:10.1029/2023EF003581, 2024.

682 Zomer, R. J., Xu, J., and Trabucco, A.: Version 3 of the global aridity index and potential
683 evapotranspiration database, Scientific Data, 9, 409, doi:10.1038/s41597-022-01493-1, 2022.